# Globally Optimal Curvature-Regularized Fast Marching for Vessel Segmentation

Wei Liao, Karl Rohr, and Stefan Wörz

University of Heidelberg, BIOQUANT, IPMB, and DKFZ Heidelberg
Dept. Bioinformatics and Functional Genomics, Biomedical Computer Vision Group

**Abstract.** We introduce a novel fast marching approach with *curvature* regularization for vessel segmentation. Since most vessels have a smooth path, curvature can be used to distinguish desired vessels from short cuts, which usually contain parts with high curvature. However, in previous fast marching approaches, curvature information is not available, so it cannot be used for regularization directly. Instead, usually *length* regularization is used under the assumption that shorter paths should also have a lower curvature. However, for vessel segmentation, this assumption often does not hold and leads to short cuts. We propose an approach, which integrates curvature regularization directly into the fast marching framework, independent of length regularization. Our approach is *globally optimal*, and numerical experiments on synthetic and real retina images show that our approach yields more accurate results than two previous approaches.

## 1 Introduction

Vessel segmentation plays an essential role in medical image analysis. For example, segmentation of retinal vessels is important for the analysis of retina images, which is crucial for the diagnosis of diseases such as diabetes. Using minimal path approaches, vessel segmentation can be formulated elegantly as *energy minimization* problems. To solve such problems, there exist *efficient algorithms*, such as Dijkstra's Algorithm ([1]) or the fast marching method (e.g., [2]), which usually allow finding the *global optimum*. Furthermore, the vessel centerlines (comprising the coordinates and order of the points) are obtained *directly*, which is an advantage compared to indirect approaches where an additional step is required after, for example, a binary segmentation. Therefore, minimal path approaches are particularly interesting for vessel segmentation.

Usually, the essential step of minimal path approaches is the outward propagation of a wavefront $\mathcal{W}$ from a start point to an end point. To determine the speed $\mathcal{F}$ of $\mathcal{W}$, there exist different strategies. In classical minimal path approaches, $\mathcal{F}$ relies on simple image features like edges (e.g., [2]), while later approaches use more elaborate intensity models (e.g., [3]). Also, additional key points can be used to adjust $\mathcal{F}$ iteratively in order to avoid problems like short cuts (e.g., [4, 5]). However, none of these approaches exploits the important geometric property that the vessels should have a smooth path. To account for the smoothness,

K. Mori et al. (Eds.): MICCAI 2013, Part I, LNCS 8149, pp. 550–557, 2013.

manually inserted key points can be used (e.g., [6]), which is time-consuming and depends strongly on the accuracy of the human operator. Alternatively, oriented filters (e.g., [7]) can be used to incorporate the smoothness automatically, but the filter orientation is quantized and integrated as additional dimension of $\mathcal{F}$, which inevitably introduces quantization errors and increases the computational effort. In [8], an iterative approach is used, where in each iteration, paths which deviate significantly from a predicted direction within a region-of-interest (ROI) are discarded. However, there is no guarantee to reach the end point. Alternatively, the approach in [9] uses the optimally oriented flux (OOF) [10] to estimate the local vessel orientation, but the OOF filter relies on image gradients, without considering the actual path geometry. In some approaches, $\mathcal{F}$ is updated dynamically to control the propagation of $\mathcal{W}$. For example, in [11, 12], the geometry of the path is used to update $\mathcal{F}$. However, there only the normal of $\mathcal{W}$ is considered. On the other hand, in [13] a longer locally back-traced path is considered, but only the appearance of the path is used to update $\mathcal{F}$, not the geometry. In addition, some of the above mentioned methods, e,g., [4, 5, 8], are not globally optimal.

In this contribution, we present a novel curvature-regularized fast marching approach for vessel segmentation. For the first time, curvature is taken into account using the *actual geometry* of vessels, instead of using the response of local filters as in [7, 9]. Furthermore, the curvature regularization is independent of length regularization. Our approach combines and extends previous approaches [11–13]: Instead of using only the normal of $\mathcal{W}$ as in [11, 12], we extract for each pixel on $\mathcal{W}$ a longer locally back-traced path $\gamma_{\text{local}}$. In addition, instead of using the appearance of $\gamma_{\text{local}}$ as in [13], we compute the curvature $\kappa$ of $\gamma_{\text{local}}$. The further propagation of $\mathcal{W}$ is controlled by *dynamically* updating $\mathcal{F}$ according to $\kappa$. Our approach is *globally optimal*, and the experiments show that we obtain significantly improved results compared to two previous approaches.

## 2 Classical Fast Marching for Vessel Segmentation

In this section, we first briefly review the classical fast marching scheme for vessel segmentation, and then we discuss the problem of length regularization.

**Energy Function.** Fast marching approaches aim at finding a path $\gamma$ between a given start point $\mathbf{x}_\text{s}$ and end point $\mathbf{x}_\text{e}$ such that an energy function is minimized. In classical approaches, the *energy function* is usually formulated as:

$$E(\gamma) := \int_\gamma \Big(\mathcal{P}(\gamma(s)) + w\Big) ds = \underbrace{\int_\gamma \mathcal{P}(\gamma(s)) ds}_{\text{data term}} + \underbrace{w \cdot \int_\gamma 1 ds}_{\text{regularization term}} , \qquad (1)$$

where $\mathcal{P}$ is a *potential function* defined based on image data, $s$ is the arc length parameter, and $w$ is a regularization constant. For many problems, it is more convenient to consider $\mathcal{P}$ as the inverse of a speed function $\mathcal{F}$, i.e., $\mathcal{P} = \frac{1}{\mathcal{F}}$. Let a wavefront $\mathcal{W}$ start at $\mathbf{x}_\text{s}$ and keep propagating outwards at the speed $\mathcal{F}$. At each

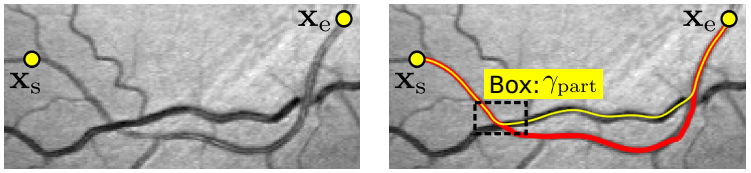


**Fig. 1.** Left: Retinal vessels crossing each other (image from DRIVE dataset [14]). Right: Segmentation results. Yellow and red colors indicate the results of a length-regularized approach [2] and our curvature-regularized approach, respectively.

position $\mathbf{x}$, the arrival time of $\mathcal{W}$ is recorded as $\mathcal{U}_{\mathbf{x}_s}(\mathbf{x})$. Upon reaching $\mathbf{x}_e$, the propagation stops, and then the minimal path $\hat{\gamma}_{\mathbf{x}_s,\mathbf{x}_e}$ is obtained with *subpixel accuracy* by a gradient descent of $\mathcal{U}_{\mathbf{x}_s}$ from $\mathbf{x}_e$ back to $\mathbf{x}_s$.

**Problem of Length Regularization.** Since $\int_\gamma 1 ds$ is the length of the path $\gamma$ [2], the regularization term in (1) assigns lower energy to shorter paths. Usually, shorter paths are assumed to have a lower curvature, so previous approaches employ *length regularization* to indirectly control the curvature of the path. However, this assumption is not always true, especially for vessels, since they often cross each other, and the shortest path found using length regularization may belong to different vessels. This problem is shown in Fig. 1: Although the red path is correct, an approach with length regularization [2] yields the yellow path, since it is shorter. With *curvature regularization*, the curvature (smoothness) of vessels can be exploited *independently* of the length regularization, so shorter paths with wrong sharp turns can be avoided. Obviously, the geometry of the path is necessary to compute the curvature. However, with previous approaches, the path geometry is usually not known until the propagation of $\mathcal{W}$ is *finished*, so a curvature regularization cannot be used with these approaches.

## 3 Curvature-Regularized Fast Marching

In this section, we first introduce a *new energy function* of minimal paths with curvature regularization, and then we show how to incorporate the curvature using a novel fast marching approach with dynamic speed.

### 3.1 New Energy Function with Curvature Regularization

Our new energy function is formulated as:

$$E(\gamma) := \int_\gamma \Big( \mathcal{P}(\gamma(s)) + \mathcal{C}(\gamma(s)) + w \Big) ds. \tag{2}$$

Compared to the energy function of the classical fast marching approaches (1), our approach includes a new term $\mathcal{C}$ which represents the curvature regularization, and which is independent of the length regularization $w$. The curvature is *not* computed over the entire path $\gamma$, but over local paths $\gamma_{\text{local}}$ of a *fixed length*

$\Gamma$ and starting at the position $\gamma(s)$ (see Fig. 2b). The function $\mathcal{C}$ can be defined using the curvature $\kappa$ of $\gamma_{\text{local}}$:

$$\mathcal{C}(\mathbf{x}) := \begin{cases} \mathcal{C}_0, & \text{if } \kappa(\gamma_{\text{local}}(\mathbf{x})) > T_\kappa, \\ 0, & \text{otherwise,} \end{cases} \tag{3}$$

where $\mathcal{C}_0$ is a large constant, and $T_\kappa$ is a threshold. Using the new energy function (2), it is now possible to avoid paths containing parts with high curvature, even if such paths may be shorter than the correct paths. For example, in Fig. 1, our approach avoids the yellow path, because it contains a part $\gamma_{\text{part}}$ with high curvature (dashed box). On the other hand, the red path does *not* contain highly curved parts. Consequently, our approach correctly finds the red path.

### 3.2 Incorporating Curvature with Dynamic Speed

**Necessity of Dynamic Speed.** As mentioned in Sec. 2, previous fast marching approaches cannot incorporate the curvature information because the geometry of the path is unknown during the propagation of $\mathcal{W}$. Furthermore, once $\mathcal{W}$ starts to propagate, $\mathcal{F}$ cannot change anymore. In order to use curvature regularization, the geometry of a local path $\gamma_{\text{local}}$ must be computed *during* the propagation of $\mathcal{W}$, and the speed $\mathcal{F}$ must be updated *dynamically* according to the curvature $\kappa(\gamma_{\text{local}})$. In other words, the propagation of $\mathcal{W}$ and the extraction of $\gamma_{\text{local}}$ must take place in an alternating manner. This can be realized by extending a fast marching approach with dynamic speed [13].

**Initial Speed.** To initialize our dynamic speed $\mathcal{F}$, we apply a commonly used speed based on the response of a multiscale vesselness filter ([15]), i.e. $\mathcal{F}(\mathbf{x}) := \mathcal{V}(\mathbf{x}) = \max_{\sigma_{\min} \le \sigma \le \sigma_{\max}} \mathcal{V}_\sigma(\mathbf{x})$, with

$$\mathcal{V}_\sigma(\mathbf{x}) = \begin{cases} 0, & \text{if } \lambda_2 > 0 \\ \exp\left(-\frac{1}{\beta^2} \cdot \frac{\lambda_1^2}{\lambda_2^2}\right)\left(1 - \exp\left(-\frac{1}{2c^2} \cdot \left(\lambda_1^2 + \lambda_2^2\right)\right)\right), & \text{otherwise,} \end{cases} \tag{4}$$

where the filter has the scale $\sigma \in [\sigma_{\min}, \sigma_{\max}]$ and its sensitivity is controlled by $\beta$ and $c$. $\lambda_1$ and $\lambda_2$ are the eigenvalues of the Hessian matrix at $\mathbf{x}$.

**Computing the Dynamic Speed.** In classical fast marching approaches, the pixel $\mathbf{x}_{\min}$ on $\mathcal{W}$ with *minimum* arrival time $\mathcal{U}_{\mathbf{x}_s}(\mathbf{x})$ is the position of wave propagation, i.e., $\mathcal{W}$ advances to the neighbors of $\mathbf{x}_{\min}$ outside $\mathcal{W}$. In our approach, we decide during the iteration whether to advance $\mathcal{W}$ or not. At $\mathbf{x}_{\min}$, we compute the curvature $\kappa(\gamma_{\text{local}})$ of a local path $\gamma_{\text{local}}$, which is extracted using gradient descent of $\mathcal{U}_{\mathbf{x}_s}$ inside $\mathcal{W}$. If $\kappa(\gamma_{\text{local}}) > T_\kappa$, then the speed $\mathcal{F}(\mathbf{x}_{\min})$ is reduced, which corresponds to the case $\mathcal{C}(\mathbf{x}_{\min}) = \mathcal{C}_0$ in (3). Consequently, $\mathcal{U}_{\mathbf{x}_s}(\mathbf{x}_{\min})$ is increased to a high value. In other words, the propagation through $\mathbf{x}_{\min}$ is slowed down. If $\kappa(\gamma_{\text{local}}) \le T_\kappa$, then $\mathcal{W}$ advances as in classical fast marching approaches, which corresponds to the case $\mathcal{C}(\mathbf{x}_{\min}) = 0$ in (3). The update *during* the propagation of $\mathcal{W}$ is the *dynamic* aspect of our speed $\mathcal{F}$. Since the new speed is not larger than the original speed, our approach satisfies the optimality criterion in [13], so the path found using our approach is *globally optimal*.

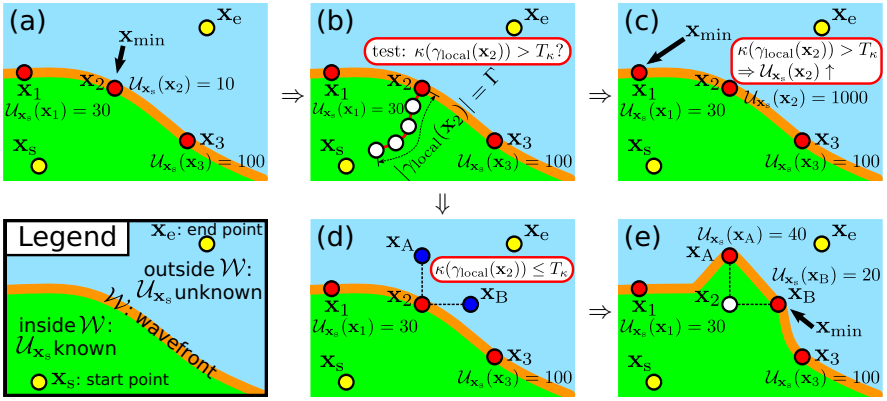


**Fig. 2.** One iteration of the wave propagation incorporating curvature regularization. (a) Select the pixel $\mathbf{x}_{\min}$ on $\mathcal{W}$ with minimum arrival time. (b) For $\gamma(s) = \mathbf{x}_2$, extract $\gamma_{\text{local}}(\mathbf{x}_2)$ with length $\Gamma$, test $\kappa(\gamma_{\text{local}})$. (c) $\kappa(\gamma_{\text{local}})$ too large: $\mathcal{F}(\mathbf{x}_2)$ is reduced and therefore $\mathcal{U}_{\mathbf{x}_s}(\mathbf{x}_2)$ increases. Select another pixel on $\mathcal{W}$. (d) $\kappa(\gamma_{\text{local}})$ small: Compute arrival time for neighbors. (e) $\mathcal{W}$ advances.

One iteration of this scheme is illustrated in Fig. 2. The wavefront $\mathcal{W}$ is shown as an orange stripe. Inside $\mathcal{W}$ (green region), $\mathcal{U}_{\mathbf{x}_s}$ is known since $\mathcal{W}$ has already visited all pixels there, but outside $\mathcal{W}$ (blue region), $\mathcal{U}_{\mathbf{x}_s}$ is unknown. Let $\mathbf{x}_1, \mathbf{x}_2, \mathbf{x}_3$ be pixels on $\mathcal{W}$ (Fig. 2a). The pixel $\mathbf{x}_{\min}$ with minimum $\mathcal{U}_{\mathbf{x}_s}$, i.e. $\mathbf{x}_2$, is considered. The steps shown in Fig. 2b and 2c are the main difference to classical fast marching approaches. Starting at $\mathbf{x}_2$, a local path $\gamma_{\text{local}}(\mathbf{x}_2)$ with a fixed length $\Gamma$ is extracted (Fig. 2b). This is possible since $\mathcal{U}_{\mathbf{x}_s}$ is known inside $\mathcal{W}$. After that, the curvature $\kappa(\gamma_{\text{local}}(\mathbf{x}_2))$ is compared with $T_\kappa$ (Fig. 2b). If $\kappa(\gamma_{\text{local}}(\mathbf{x}_2)) > T_\kappa$, then $\mathcal{F}(\mathbf{x}_2)$ should be reduced, and $\mathcal{U}_{\mathbf{x}_s}(\mathbf{x}_2)$ re-computed, while $\mathcal{W}$ does *not* change (Fig. 2c). Obviously, $\mathcal{U}_{\mathbf{x}_s}(\mathbf{x}_2)$ increases, so the propagation through $\mathbf{x}_2$ (with $\gamma_{\text{local}}(\mathbf{x}_2)$ having high curvature) is slowed down. If $\kappa(\gamma_{\text{local}}(\mathbf{x}_2)) \leq T_\kappa$, then we proceed as in classical fast marching approaches: The neighbors of $\mathbf{x}_2$ outside $\mathcal{W}$, i.e., $\mathbf{x}_A$ and $\mathbf{x}_B$, are found (Fig. 2d) and $\mathcal{W}$ advances to $\mathbf{x}_A$ and $\mathbf{x}_B$, while $\mathbf{x}_2$ is moved into the inside of $\mathcal{W}$ (Fig. 2e). In either case, the pixel on $\mathcal{W}$ with minimum $\mathcal{U}_{\mathbf{x}_s}$ value, i.e., $\mathbf{x}_{\min}$, will be considered in the next iteration.

## 4 Experimental Results

We carried out experiments using synthetic images and retina images on a PC with a 2.27 GHz CPU and 3 GB memory, and compared our approach with two previous approaches: The classical fast marching approach using the vesselness measure [15] as speed (Classical FM), and the intensity-based approach in [3] (Li-Yezzi FM). Most parameter values are fixed for all data, empirically determined based on one image: $w = 1, \mathcal{C}_0 = 10^7, \sigma_{\min} = 1, \sigma_{\max} = 2, \beta = 0.5, c = 0.5$. $\Gamma$ and $T_\kappa$ typically have values of 10 and 0.2, respectively. Our algorithm is relatively robust to the choice of parameter values.

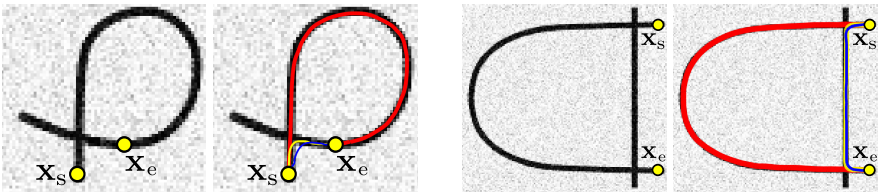


**Fig. 3.** Results on synthetic images. The yellow, blue and red lines show the results of Classical FM, Li-Yezzi FM, and our approach, respectively.

**Synthetic Images.** We tested our approach with different synthetic images. For example, Fig. 3 shows a loop, as well as a curve which crosses a straight line. In both cases, our approach yields the paths with low curvature (red lines), even though these paths are much longer than the short cuts. In contrast, both Classical FM and Li-Yezzi FM result in short cuts.

**Retina Images.** We have used all 40 retina images of the DRIVE dataset [14] for evaluation. For *each* image, one to three vessels which *cross* other vessels are selected, resulting in 81 vessels in total. Such vessels are very common in retina images. The results for four vessels are shown in Fig. 4. In the first row, the vessel crosses another vessel which has a similar radius. There, Classical FM results in a short cut with high curvature, while our approach finds the correct path. Li-Yezzi FM also finds the correct path, because the intensity of the vessel is quite different from the other vessel. However, as shown in the second row, the intensity is not a good feature, since the intensities inside the vessel vary significantly. As a result, the Li-Yezzi FM approach runs into a neighboring vessel, while Classical FM and our approach yield the correct path. For the vessel in the third row, Classical FM and Li-Yezzi FM both yield short cuts. In contrast, our approach achieves the correct path in this case, as well as in the fourth row, which shows an even more difficult case: The correct vessel is much longer than the short cuts.

For a quantitative evaluation, we compared the results of our approach and the two previous approaches with the ground truth provided in the DRIVE dataset. The ground truth is a binary segmentation of all pixels corresponding to vessels, while the results from fast marching approaches are centerlines with subpixel accuracy. To enable a comparison, we determine the set $\mathcal{S}_0$ of pixels which lie on the path of the segmented centerline, and the set $\mathcal{S}_1$, which is given by the pixels of $\mathcal{S}_0$ inside the vessel in the binary segmentation. The quotient $Q_{\text{inside}} = \frac{|\mathcal{S}_1|}{|\mathcal{S}_0|}$ is used to measure the accuracy of the segmented centerlines. The results and run time for the four vessels in Fig. 4 as well as the mean values for all 81 vessels are summarized in Table 1. It can be seen that our approach yields significantly higher values for $Q_{\text{inside}}$ compared to Classical FM and Li-Yezzi FM (e.g., 99.13% on average, compared to 45.27% and 48.18% for previous approaches). Additionally, a lower mean run time of 0.68 s compared to 0.79 s (Li-Yezzi FM) is achieved.

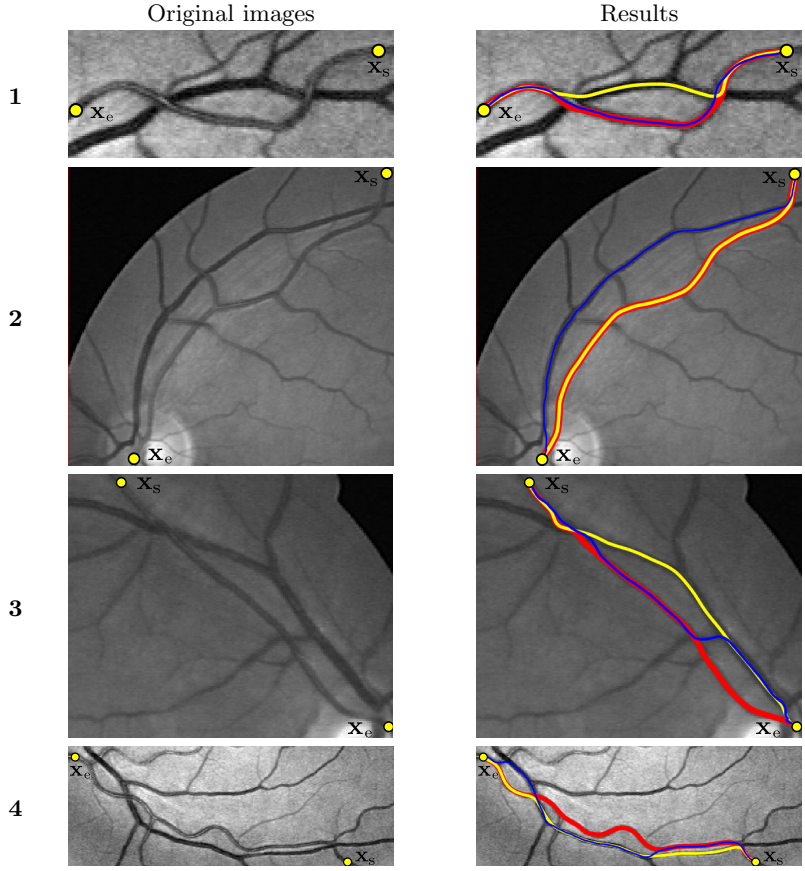


**Fig. 4.** Results for four vessels from the DRIVE dataset. The yellow, blue and red lines show the results of Classical FM, Li-Yezzi FM, and our approach, respectively.

**Table 1.** Comparison of quantitative results for retinal vessels

| Vessel | Classical FM | | Li-Yezzi FM | | **Our approach** | |
|---|---|---|---|---|---|---|
| | $Q_{\text{inside}}$ | Time | $Q_{\text{inside}}$ | Time | $Q_{\text{inside}}$ | Time |
| 1 | 54.90% | 0.08 s | 94.04% | 0.17 s | 94.55% | 0.26 s |
| 2 | 100.00% | 0.39 s | 11.49% | 2.76 s | 100.00% | 0.88 s |
| 3 | 26.42% | 0.19 s | 67.49% | 0.79 s | 99.61% | 0.63 s |
| 4 | 31.96% | 0.31 s | 42.78% | 1.41 s | 99.42% | 0.96 s |
| Mean for all 81 | 45.27% | 0.22 s | 48.18% | 0.79 s | 99.13% | 0.68 s |

## 5 Discussion and Conclusions

We presented a novel globally optimal fast marching approach for vessel segmentation with curvature regularization. The fast marching method can be interpreted as the propagation of a wavefront. *During* the propagation, we

dynamically update the speed of the wavefront according to the curvature of local paths, in order to avoid erroneous segmentation results which are shorter but have higher curvature. Experimental results on synthetic and retina images show that using our approach, short cuts with high curvature can be effectively avoided, and therefore our approach yields better results, in particular, for vessels which cross other vessels. Although our approach involves additional computation of the curvature, it is more efficient than a previous approach [3].

**Acknowledgment.** Support of the Deutsche Forschungsgemeinschaft (DFG) within the project QuantVessel (RO 2471/6) is gratefully acknowledged.

## References

1. Dijkstra, E.: A Note on Two Problems in Connection with Graphs. Numerische Mathematik, 269–271 (1959)
2. Cohen, L., Kimmel, R.: Global Minimum for Active Contour Models: A Minimal Path Approach. Internat. J. of Computer Vision 24, 57–78 (1997)
3. Li, H., Yezzi, A.: Vessels as 4-D Curves: Global Minimal 4-D Paths to Extract 3-D Tubular Surfaces and Centerlines. IEEE TMI 26, 1213–1223 (2007)
4. Benmansour, F., Cohen, L.: Fast Object Segmentation by Growing Minimal Paths from a Single Point on 2D or 3D Images. J. of Math. Imag. Vis. 33, 209–221 (2009)
5. Kaul, V., Yezzi, A., Tsai, Y.: Detecting Curves with Unknown Endpoints and Arbitrary Topology Using Minimal Paths. IEEE TPAMI 34, 1952–1965 (2012)
6. Poon, K., Hamarneh, G., Abugharbieh, R.: Live-Vessel: Extending Livewire for Simultaneous Extraction of Optimal Medial and Boundary Paths in Vascular Images. In: Ayache, N., Ourselin, S., Maeder, A. (eds.) MICCAI 2007, Part II. LNCS, vol. 4792, pp. 444–451. Springer, Heidelberg (2007)
7. Pechaud, M., Keriven, R., Peyre, G.: Extraction of Tubular Structures Over an Orientation Domain. In: Proc. CVPR 2009, Miami, FL/USA, vol. 1, pp. 336–342 (2009)
8. Lo, P., van Ginneken, B., de Bruijne, M.: Vessel Tree Extraction Using Locally Optimal Paths. In: Proc. ISBI 2010, Rotterdam, The Netherlands, pp. 680–683 (2010)
9. Benmansour, F., Cohen, L.D.: Tubular Structure Segmentation Based on Minimal Path Method and Anisotropic Enhancement. Int. J. of Computer Vision 92, 192–210 (2011)
10. Law, M., Chung, A.: Three Dimensional Curvilinear Structure Detection Using Optimally Oriented Flux. In: Forsyth, D., Torr, P., Zisserman, A. (eds.) ECCV 2008, Part IV. LNCS, vol. 5305, pp. 368–382. Springer, Heidelberg (2008)
11. Parker, G., Wheeler-Kingshott, C., Barker, G.: Estimating Distributed Anatomical Connectivity Using Fast Marching Methods and Diffusion Tensor Imaging. IEEE Trans. on Medical Imaging 21, 505–512 (2002)
12. Joshi, V., Garvin, M., Reinhardt, J., Abramoff, M.: Identification and Reconnection of Interrupted Vessels in Retinal Vessel Segmentation. In: Proc. ISBI 2011, Chicago, IL/USA, pp. 1416–1420 (2011)
13. Liao, W., Wörz, S., Rohr, K.: Globally Minimal Path Method Using Dynamic Speed Functions Based on Progressive Wave Propagation. In: Lee, K.M., Matsushita, Y., Rehg, J.M., Hu, Z. (eds.) ACCV 2012, Part II. LNCS, vol. 7725, pp. 25–37. Springer, Heidelberg (2013)
14. Staal, J., Abramoff, M., Niemeijer, M., Viergever, M., van Ginneken, B.: Ridge based vessel segmentation in color images of the retina. IEEE Trans. on Medical Imaging 23, 501–509 (2004)
15. Frangi, A., Niessen, W., Vincken, K., Viergever, M.: Multiscale vessel enhancement filtering. In: Wells, W.M., Colchester, A.C.F., Delp, S.L. (eds.) MICCAI 1998. LNCS, vol. 1496, pp. 130–137. Springer, Heidelberg (1998)